



HAL
open science

Impact of baculoviral transduction of fluorescent actin on cellular forces

Sara Bouizakarne, Jocelyn Etienne, Alice Nicolas

► **To cite this version:**

Sara Bouizakarne, Jocelyn Etienne, Alice Nicolas. Impact of baculoviral transduction of fluorescent actin on cellular forces. *European Journal of Cell Biology*, 2023, 102 (2), 10.1016/j.ejcb.2023.151294 . hal-03971453

HAL Id: hal-03971453

<https://hal.science/hal-03971453v1>

Submitted on 3 Feb 2023

HAL is a multi-disciplinary open access archive for the deposit and dissemination of scientific research documents, whether they are published or not. The documents may come from teaching and research institutions in France or abroad, or from public or private research centers.

L'archive ouverte pluridisciplinaire **HAL**, est destinée au dépôt et à la diffusion de documents scientifiques de niveau recherche, publiés ou non, émanant des établissements d'enseignement et de recherche français ou étrangers, des laboratoires publics ou privés.



Distributed under a Creative Commons Attribution - NonCommercial - NoDerivatives 4.0 International License

Impact of baculoviral transduction of fluorescent actin on cellular forces

Sara Bouizakarne^{a,b}, Jocelyn Etienne^b, Alice Nicolas^a,

^a*Univ. Grenoble Alpes, CNRS, LTM, 38000 Grenoble, France*

^b*Univ. Grenoble Alpes, CNRS, LIPHY, 38000 Grenoble, France*

Abstract

Live staining of actin brings valuable information in the field of mechanobiology. Gene transfer of GFP-actin has been reported to disturb cell rheological properties while gene transfer of fluorescent actin binding proteins was not. However the influence of gene transfer on cellular forces in adhered cells has never been investigated. This would provide a more complete picture of mechanical disorders induced by actin live staining for mechanobiology studies. Indeed, most of these techniques were shown to alter cell morphology. Change in cell morphology may in itself be sufficient to perturb cellular forces. Here we focus on quantifying the alterations of cellular stresses that result from baculoviral transduction of GFP-actin in MDCK cell line. We report that GFP-actin transduction increases the proportion of cells with large intracellular or surface stresses, especially in epithelia with low cell density. We show that the enhancement of the mechanical stresses is accompanied by small perturbations of cell shape, but not by a significant change in cell size. We thus conclude that this live staining method enhances the cellular forces but only brings subtle shape alterations.

Keywords: baculoviral transduction, actin, mechanical stresses, traction force microscopy, intracellular stress microscopy

1. Introduction

Ample evidence shows that cellular forces are part of the regulation scheme of many signaling pathways of adherent cells. For instance, cell adhesion builds in relation to mechanical forces, either from intracellular origin or from the extracellular environment (Iwamoto and Calderwood, 2015; Riveline et al., 2001). Cell migration is also based on the fine tuning of adhesion dynamics, actin flows and mechanical stresses (Yamaguchi et al., 2022). Stem cell differentiation was shown to involve tensions from the acto-myosin cytoskeleton too (Dupont et al., 2011; Wickström and Niessen, 2018).

Cellular forces that originate from the actin cytoskeleton have attracted much attention and the translation of biochemical signaling to mechanical forces (and the reciprocity) has become part of mechanistic analysis (Roca-Cusachs et al., 2017; Evers et al., 2021). In this context, actin staining of live cells is a valuable tool that allows correlating cellular forces to actin organization (Prager-Khoutorsky et al., 2011; Murrell et al., 2015). Different staining techniques are available, each of them showing advantages and drawbacks in term of actin visualization (Melak et al., 2017). Notably, alterations in actin organization and cell functioning were reported for all of them. For instance actin fused with fluorescent protein and actin-binding proteins were shown to label different subpopulations of F-actin (Belin et al., 2014). In addition, actin-GFP was reported to stiffen the cytoskeleton (Deibler et al., 2011; Sliogeryte et al., 2016). Furthermore, in a reconstituted system using myosin head fragments coated on coverglass surfaces, the GFP-actin filaments were shown to bind to motor proteins but without being able to slide on the coverglass in contrast to untagged actin filaments (Aizawa et al., 1997). Actin-binding proteins also showed an impact on cell mechanics (Flores et al., 2019). For instance, LifeAct was reported to disturb stress fiber dynamics, as well as the content of vimentin and tubulin. LifeAct transduced cells were also shown to be softer and more viscous than the control cells (Flores et al., 2019), thus exhibiting opposite rheological

perturbation compared to actin-GFP transduced or transfected cells (Pravincumar et al., 2012; Sliogeryte et al., 2016).

Thus several studies evidenced that live actin staining has an impact on cell morphology and the mechanical properties of the cell body. Cell mechanical properties are intimately linked to actin organization, and their perturbation could be understood in terms of the remodeling of the cytoskeleton (Pravincumar et al., 2012; Sliogeryte et al., 2016; Nagasaki et al., 2017; Flores et al., 2019). Alteration of cell shape or of cell rheological properties are also expected to influence stress generation in cells (Oakes et al., 2014). However, the link between cell stiffness and cellular stresses is far from obvious. For instance the thickness of actin fibers is not a determinant of the level of cellular forces (Murrell et al., 2015; Oakes et al., 2018). It remains therefore an open question whether cell contractility is affected by actin live staining as well as cell stiffness. In order to address this question, we set up a direct measure of cell mechanical stresses and assessed perturbation from the actin live staining. In this work, cell traction forces and intracellular stresses were quantified by the means of Traction Force Microscopy (TFM) (Butler et al., 2002) and Intracellular Stress Microscopy (ISM) (Moussus et al., 2014a). We focused on epithelial cells, using Martin Darbin Canine Kidney (MDCK) cell line as a model system. Baculoviral vector for GFP-actin gene delivery was used to transiently stain actin in living cells (Hu, 2008; Liu et al., 2014). Baculovirus is an insect virus whose genes promoters are not recognized in mammal cells and that demonstrated a good compromise between the efficacy of gene delivery and a limited toxicity compared to other techniques of gene delivery (Chen et al., 2011).

Using this model system, we analyzed the effect of GFP-actin baculoviral transduction on the forces exerted by cell layers at densities that are relevant for the epithelial model. Since techniques quantifying forces exerted by cells make use of the measure of the deformation of the underlying soft substrate, we first evaluated the efficacy of the transduction of MDCK cells as a function of the stiffness of the substrate. Collagen I-coated polyacrylamide hydrogels were used as soft matrices. We then assessed the influence of the transduction on cell proliferation on these soft gels. The sensitivity of cell morphological parameters and of cellular stresses to the expression level of fluorescent actin was analyzed, and disturbance in the relationship between cell area and forces coming from GFP-actin baculoviral transduction was quantified. Taken together, our observations show that baculoviral GFP-actin transduction only slightly perturb cell shape but causes larger traction forces on the extracellular matrix, independent of the level fluorescent actin.

2. Material and Methods

2.1. Gel preparation

Cells were cultured on polyacrylamide hydrogels coated with collagen I. The polyacrylamide hydrogels were prepared as described in (Palva et al., 2020). In brief, a UV sensitive solution of 10% – 0.5% solution of acrylamide – N,N-methylene-bis-acrylamide (Bio-Rad, Marnes-la-Coquette, France) containing 0.2% of UV-sensitive initiator Irgacure 819 (Ciba Specialty Chemicals, Basel, Switzerland) and 0.01% of propylamine (Sigma-Aldrich, Saint Quentin Fallavier, France) was prepared. 0.22% *v/v* of 200 nm far red fluorescent beads (2% solid beads, F8807 Molecular Probes, Life Technology SAS, Courtaboeuf, France) were added to the precursor solution as fluorescent trackers of the deformation of the hydrogel (Mgharbel et al., 2022). The hydrogels were polymerized on 24 mm glass coverslips coated with Bind-Silane (GE Healthcare, New York, USA) to ensure a covalent binding of the gel to the coverslip (Palva et al., 2020). A droplet of 24 μ L of the precursor solution was deposited on the coverslip and covered by a transparent microscope glass slide treated with a fluorinated hydrophobic silane as described in (Palva et al., 2020). The solution was then exposed to UV-A (Eleco UVP281, Gennevilliers, France, 2W/cm²) for few seconds and immediately rinsed 3 times in deionized water. As described in (Palva et al., 2020), the duration of the UV exposure controls the stiffness of the hydrogel. 3.5 ± 0.4 kPa (resp. 61.8 ± 2.2 kPa) gels were obtained with 8 s (resp. 50 s) exposure time. The gels were then let for swelling overnight. The thickness of the gels was of the order of 30 μ m.

The stiffness of the hydrogels was characterized using Atomic Force Microscopy (NanoWizard II, JPK Instruments, Berlin, Germany) in the force mapping mode with MLCT C tip cantilevers (Bruker, Palaiseau, France) of nominal spring constant of 0.01 N/m. Indentation curves were fitted using Hertz-Sneddon model.

As polyacrylamide hydrogels are not permissive to cell adhesion, the surface of the hydrogels was coated with Collagen I from rat tail (Reference C3867, Sigma-Aldrich, Saint Quentin Fallavier, France). The coating was performed as follow. The gels were first dehydrated under a sterile hood for 1 h. 500 μL of a solution of the diazine-NHS crosslinker Sulfo-LC-SDA (Pierce, Thermo Fisher Scientific, Gennevilliers, France) freshly dissolved in deionized water at 0.6 mg/mL was then added on top of every hydrogel. After 2 h, the solution was removed and the hydrogels were let to dehydrate for 1 h. They were then exposed to UV-A for 5 min (Eleco UVP281, Gennevilliers, France, $2\text{W}/\text{cm}^2$) to crosslink the diazine group to polyacrylamide. 500 μL of a solution of Collagen I diluted in deionized water at concentration 9 $\mu\text{g}/\text{mL}$ was added on top of the hydrogels. The solution was then evaporated, leading to the deposition and theoretical crosslinking of 1 $\mu\text{g}/\text{cm}^2$ of Collagen I to the surface of the hydrogels. Functionalized hydrogels were then stored at 4°C and used within 1 month. Surface coating was controlled as described in (Palva et al., 2020) using Alexa Fluor 488 conjugated Collagen I polyclonal antibody (Reference bs-10423R-A488, Cliniscience, Nanterre, France). Before use, the gels were rehydrated in PBS+/+ (Gibco, Thermo Fisher Scientific, Gennevilliers, France) for 24 h at 4°C . 1 h before cell seeding, PBS was replaced by the culture medium and the gels were placed at 37°C .

2.2. Preparation of glass substrates

Collagen I-coated glass coverslips were used as control. The coverslips were soaked in a solution of 0.1 M of NaOH for 10 min, and extensively rinsed in deionized water. They were then rinsed with ethanol and dried with dry air. 200 μL of a solution composed of 484 μL of acetic acid, 56 μL of Bind-Silane (PlusOne, VWR, Rosny-sous-Bois, France) and completed up to 15 mL with absolute ethanol was spread on the coverslip and wiped off with a dust free wiper. Covalent binding of Collagen I was then performed as done on hydrogels, using Sulfo-LC-SDA as a crosslinker.

2.3. Cell culture and GFP-actin transduction

All the products cited below were purchased from Thermo Fisher Scientific, Gennevilliers, France. MDCK (NBL-2) cells were purchased from ATCC (ATCC-CCL-34, LGC Standards, Molsheim, France). The cells were grown in a Dulbecco's Modified Eagle Medium (DMEM) with high glucose and GlutaMAX supplement, 10% fetal bovine serum (FBS) and 1% antibiotic-antimycotic. Cells were incubated in 5% CO_2 and 37°C . They were passaged at 60%-80% confluency by washing them using PBS-/- for 5 min, then detached with 0.05% Trypsine-EDTA for 8 min. GFP-actin transduction was performed using CellLight actin-GFP, BacMam 2.0 (Reference C10582). The cells were seeded on the substrate (glass or soft hydrogel) at given cell densities and incubated for 6 h. CellLight actin-GFP was added directly in the medium at a concentration of 50 – 70 virus particles/cell. The cells were then agitated at 50 rpm for 19 h at 5% CO_2 and 37°C . Culture medium was then changed and the cells used for experiments. The control, non transduced, cells were also submitted to 19 h of smooth agitation.

Cells were initially seeded at a density of 60000 cells/ cm^2 for the proliferation and the stiffness sensitivity assays. Image acquisition was started 1 h after changing the culture medium. Cells were seeded at 60000, 80000 and 100000 cells/ cm^2 for the cellular stress experiments to analyze the effect of cell density. Image acquisition was started 2 h after changing the culture medium for these experiments.

2.4. Image acquisition

Images were obtained from an inverted microscope (IX83 Olympus, Olympus France, Rungis, France) equipped with a temperature- and CO_2 -controlled incubation chamber (Okolab, Rovereto, Italy) and a ORCA-Flash4.0 camera (Hamamatsu Photonics, France). Cell proliferation assays were performed using 20 X magnification (NA 0.8). Stacks of images with 0.5 μm z-interval were acquired in phase contrast and

GFP channels. These stacks were used to properly identify cell nuclei and to visualize cell contours, both requiring images at different heights in the cell. Images to compare the expression level of the transduced cells in dependence on the stiffness were obtained by imaging 4 independent experiments with identical illumination and exposure parameters. Cell proliferation assay was performed by sequential imaging of field of views (6 per well). Image acquisition for TFM analysis was performed using a 60 X oil immersion objective (NA 1.4). Stacks of images of the fluorescent beads were acquired at the bottom and at the surface of the hydrogel with $0.3 \mu\text{m}$ spacing. Stacks of phase contrast and GFP images were performed at the surface of the hydrogel with spacing of $0.5 \mu\text{m}$. The use of images stacks is described below.

2.5. Image analysis

To assess cell proliferation or cell density, cells were counted manually on phase contrast stacks using ImageJ software (v 1.53, NIH, USA). The z-stacks were used to locate cell nuclei and to draw cell contours as shown on Figures S1 and S2. Expression level of transduced cells was obtained by sum-projecting the GFP stacks. A mask was manually drawn for each fluorescent cell from the projected image. The contrast of the raw image was kept unchanged, and contours were drawn for all the cells which intensity would emerge from the background noise. Cell area and intensity level were obtained with ImageJ Measure tool. As all the images were acquired in identical imaging conditions, data from independent experiments could be pooled for further statistical analysis and experiments from different stiffness conditions could be compared.

Cell contours were also drawn manually on phase contrast stacks of images for cellular stress analysis. Here, only cell contact area with the polyacrylamide hydrogel was of interest, as it was used to segment the stress fields with the cells. GFP images were used to check the contours of the transduced cells and allowed to confirm the reliability of the contours drawn on phase contrast imaging (Figure S2). It is to be noted that cell contours at the basal surface of the cells may differ from the contours visible at a higher altitude, away from the gel surface. Importantly, this technique allowed to account for cryptic lamellipodia (Fig. S3).

2.6. Quantification of the cellular forces

Quantification of the deformation field of the hydrogel is described elsewhere (Mgharbel et al., 2022). In brief, the deformation field is obtained by measuring the displacement of fluorescent beads at the surface of the hydrogel by reference to a cell-free hydrogel. To this end, the cells were removed at the end of the experiment using 0.5% trypsin-EDTA (Gibco, Thermo Fisher Scientific, Gennevilliers, France reference 15400) for 2 h. Reference images at the bottom of the hydrogel and at the top surface were selected from the reference stacks. A home-made registration algorithm described elsewhere (Mgharbel et al., 2022) was used to select images with the best correlation in the stacks acquired in the presence of the cells. Since the cells were covering the field of view, the top surface of the hydrogel was not showing undeformed regions that could be used to correct for unintentional in-plane drifts. Registration was thus performed on the images taken at the bottom of the hydrogel, as close as possible to the glass coverslip on which the hydrogel is covalently bound. It was then propagated to the images of the fluorescent beads at the top surface of the hydrogel (Moussus et al., 2014a).

Once the images were corrected from drifts, the deformation field was quantified using Kanade–Lucas–Tomasi optical flow algorithm as described in (Mgharbel et al., 2022). This algorithm makes a pyramidal detection of flows of the intensity averaged on interrogation windows. The displacement field is iteratively calculated on the different levels of the pyramid, that show increased resolution (Lucas and Kanade, 1981). Here 15000 fluorescent beads were used to track the displacement field on images whose size is of order of 2000×2000 pixels. Four levels in the pyramid were used, thus beginning with low resolution images whose pixel size is 16 times larger than in the original images. The interrogation windows used to track the displacements were of 30×30 pixels for all levels of the pyramid.

We then used two different read-outs to characterize the cellular active stresses: the traction forces evaluated by TFM and a direct read-out of substrate deformation, based on areal strain. As described below, the latter provides information on cell contractility.

Fast Fourier transform (FFT) (Butler et al., 2002) was used to calculate the surface stresses the cells transmit to the extracellular matrix, denoted \mathbf{f} . As the cells were covering most of the field of view, the zero force boundary condition required for TFM calculation could not be fulfilled. As shown in (Hur et al., 2012; Tambe et al., 2013), this limitation which induces wrong force estimates can be resolved by removing from the analysis a corona at the edge of the image. Here a 25 μm wide corona was withdrawn. Median values of the magnitude of \mathbf{f} out of the corona, either at the cell scale or at the experiment scale were used to compare conditions.

Areal strain ϵ_a on the other hand was directly evaluated from the measurement of the in-plane components $u_{x,y}$ of the displacement field at the upper surface of the substrate, $\epsilon_a = \partial_x u_x + \partial_y u_y$, with x and y a coordinate system in this plane and ∂_x and ∂_y the partial derivatives relative to x and y . Areal strain can be related to the intracellular stresses calculated using Intracellular Stress Microscopy (Moussus et al., 2014a). This method assumes that the cells are bound to the extracellular matrix and thus that the in-plane deformation field on the top of the matrix is identical to the in-plane deformation at the basal surface of the cells (see (Moussus et al., 2014b; Delanoë-Ayari et al., 2022) concerning the relevance of this assumption). This allows to quantify the internal strain of the cells as long as cellular stresses are transmitted to the basal membrane (Delanoë-Ayari et al., 2022). This quantity thus informs on cell contractile and tensile capabilities independent of the biochemical mechanism at play. The proper quantification of the intracellular stresses requires the knowledge of the cell Young’s modulus. As we do not know it, we focus on the cellular strains. The latter are proportional to the stresses, the coefficient of proportionality being the Young’s modulus. Cellular strains were then quantified by the in-plane differentiation of the displacement field at the surface of the hydrogel, following (Moussus et al., 2014a):

$$\epsilon_c = \begin{pmatrix} \epsilon_{xx} & \epsilon_{xy} \\ \epsilon_{xy} & \epsilon_{yy} \end{pmatrix}$$

$$\text{with } \begin{cases} \epsilon_{xx} = \frac{1}{1-\nu_c} \left(\frac{\partial u_x}{\partial x} + \nu_c \frac{\partial u_y}{\partial y} \right) \\ \epsilon_{yy} = \frac{1}{1-\nu_c} \left(\frac{\partial u_y}{\partial y} + \nu_c \frac{\partial u_x}{\partial x} \right) \\ \epsilon_{xy} = \frac{1}{2(1+\nu_c)} \left(\frac{\partial u_x}{\partial y} + \frac{\partial u_y}{\partial x} \right) \end{cases} \quad (1)$$

where ν_c is the Poisson’s ratio of the cell material, taken as 0.5 (Moussus et al., 2014a). We then find that $\epsilon_a = (1 - \nu_c)\text{tr}(\epsilon_c)$, which allows to relate the two approaches and analyze cell contractile capabilities by the measure of the areal strain. The areal strain can thus be interpreted as the local cell deformations in a gedanken experiment in which adherent cells would move from a relaxed to a tensed state.

2.7. Statistical analysis

Two to four independent experiments were conducted, as specified in the Result section. Independent experiments were consisting of cells from different passage numbers or from different batches. Each experiment was multiplexed in 1 to 2 wells for each condition (control or transduction). Several fields of view were captured in each well (from 4 to 6). Median values were calculated for data coming from the same experiment and the means of the medians were compared in between conditions. Significance between the means was assessed by performing Student pair tests. Effects of the different stiffnesses were compared by using one way-ANOVA tests. In order to evaluate monotonic relations between two parameters (e.g. f and cell area or f and the intensity per unit surface of the GFP) Spearman’s rank correlation tests were performed. Outputs from control and transduced cells in relation to cell area were compared by sampling the data on identical bins. The average and the standard deviation were obtained for each bin. The mean values of the control and transduction conditions were then subtracted in all bins

and the difference was tested against a random normal distribution centered on the mean (or on zero) (Student t-test) or a correlation was investigated (Spearman’s rank correlation test). Distributions of the outputs from control and transduction experiments were compared using two sample Kolmogorov-Smirnov test (noted KS test hereafter).

Finally, correlation of cellular stresses or morphological parameters with the expression level of GFP-actin was addressed for each field of view with Spearman’s rank correlation test. Medians and quartiles of the p-values were used to assess the existence of a correlation. This protocol was imposed by the fact that the different experiments on cellular stresses did not have a shared reference for the intensity level.

The statistic tests were performed with Matlab (v7.10 2010) and Libre Office Calc (v6.4.7.2).

3. Results

3.1. *The efficacy of GFP-actin transduction is sensitive to the stiffness of the extracellular matrix but the expression level is not*

MDCK cells were seeded on 3.5 kPa (soft), 61 kPa (stiff) collagen I-coated polyacrylamide hydrogels and on collagen I-coated glass with the same surface density of collagen I for all conditions (Palva et al., 2020). The cells were transduced for GFP-actin respectively on the hydrogels and on the glass, as described in Material and Methods. After 19 h, the transduction medium was withdrawn and replaced by culture medium. The cells were then counted on the phase contrast images, taking advantage of the in-depth view provided by the stacks of images that allowed to identify cell nuclei (Fig. S1). In the same way, fluorescent cells were counted on the GFP images. For those, the stack of images was projected to a unique image, which allowed to clearly visualize cell nuclei and contours (Fig. S1). As explained in the Material and Methods section, cells were counted as expressing GFP-actin as soon as their intensity signal would emerge from the background. From this analysis, we observed differences in the global intensity level of GFP-actin between the soft and the stiff or the glass conditions (Fig. 1). We asked whether this observation was imputable to the lower number of cells on the soft substrate. Indeed, cell proliferation is expected to be stiffness-dependent (Wang et al., 2000). However, while we have consistently observed a reduced number of cells on the soft hydrogel (Fig. 1D), the ratio of fluorescent cells to total cells showed that soft hydrogels were bearing a larger proportion of fluorescent cells (Fig. 1E). The stiff and the glass conditions were nevertheless not providing significantly different results. We then focused on the level of GFP-actin expression per cell in relation with the stiffness. The expression level was assessed by the intensity of the fluorescent cells per unit of their area. As described in Material and Methods, care was taken to keep identical parameters for the image acquisition and analysis. The intensity per unit area did not show any significant sensitivity to stiffness (Fig. 1F), meaning that while the efficacy of GFP-actin transduction is stiffness sensitive, the expression level of GFP-actin is not.

3.2. *Proliferation is delayed by gene transfer*

We then addressed whether cell growth is affected by gene transfer. These experiments were conducted for the soft condition (3.5 kPa). Since we are interested in measuring the impact of actin staining on cell mechanical stresses, and specifically using commercial baculoviral transduction, we chose to compare the transduced condition to cells that had not been exposed to the transduction medium. These control cells were grown in parallel to those exposed to the transduction medium as described in Material and Methods. While both the control population and the one exposed to the transduction medium were increasing in time, monitored from the end of the transduction 20 h post seeding (Fig. 2A), the transduced condition was lagging compared to the control. Figure 2B shows that the difference of the cell densities in time is stable around a mean value, cells being more numerous in the control than in the transduced condition (Student test, $p = 0.001$). This suggests that both populations statistically grow at the same rate but that the 19 h transduction process has arrested proliferation or killed cells compared to control. We also asked whether MDCK cells would keep GFP-actin expression after cell division. We found that from 20 h post seeding to 35 h, the number of fluorescent cells did not vary in a statistically significant way (Student

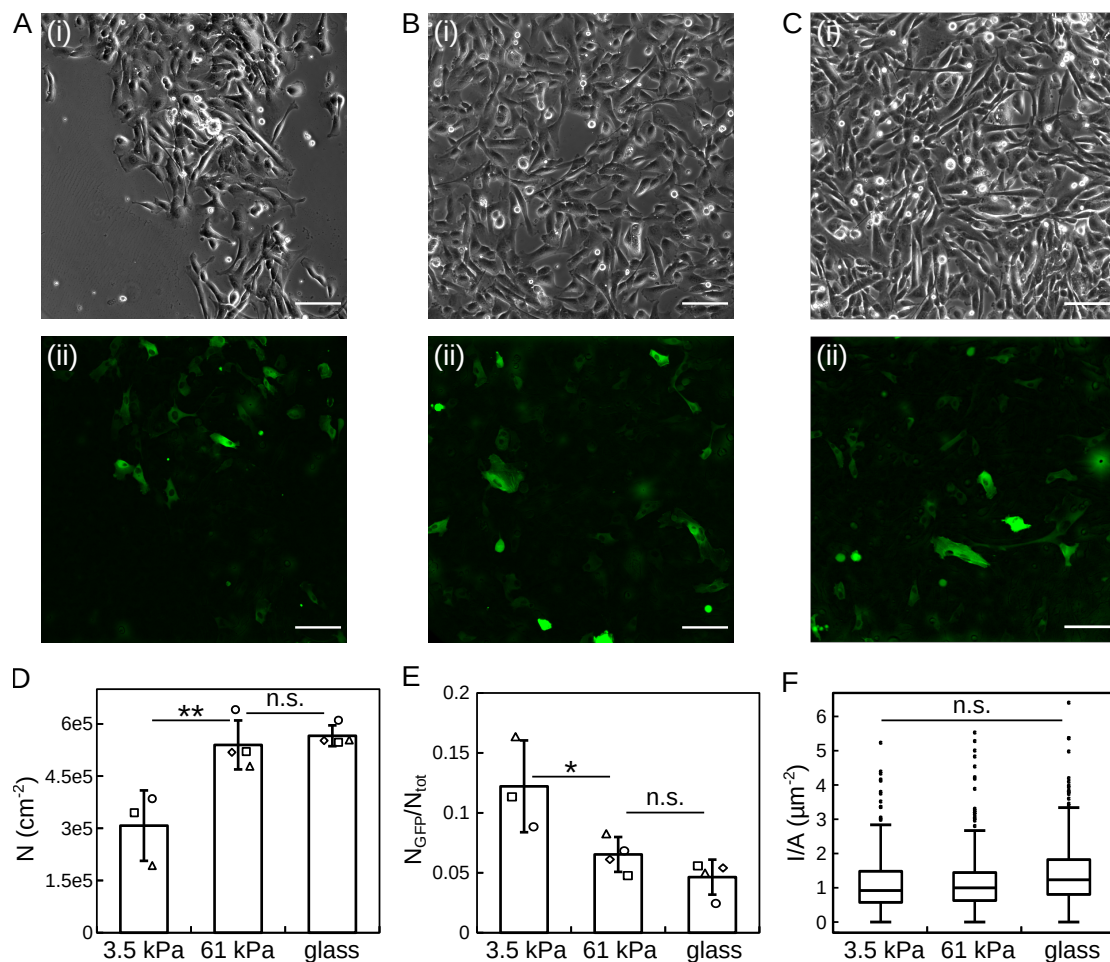


Figure 1: Stiffness-sensitivity of the transduction. (A-C)(i) Phase contrast images of GFP-actin transduced MDCK cells cultured on collagen I-coated polyacrylamide hydrogels of (A) 3.5 kPa, (B) 61 kPa and (C) on collagen I-coated glass. (A-C)(ii) Fluorescence signal of GFP-actin. Bars = 100 μm . (D) Cell density 20 h post seeding is stiffness sensitive ($p = 0.009$ and $p = 0.15$). (E) The relative ratio of fluorescent cells is larger on the soft hydrogels ($p = 0.04$ and $p = 0.10$). (F) The intensity of fluorescence per unit surface of the transduced cells is not sensitive to the stiffness (Anova test, $p = 0.3$). *, **, *** and n.s. denote respectively $p < (0.05, 0.01, 0.001)$ and non significant ($n=4$, cell numbers are 4026, 9415 and 9874 for 3.5 kPa, 61 kPa and glass). Bars are the standard deviation of the repeats in D–E, and the symbols show the medians of the independent experiments. Identical symbols show paired experiments. The boxes in F delineates the 25th and 75th percentiles with the central line showing the median, and the bars encompass 99.3% of the data around the median.

test around the mean, $p = 1$) (Fig. 2C). The decrease in the mean cell number from 26 h to 44 h was not statistically significant (Spearman’s rank correlation test: $p = 0.08$). This led to the conclusion that GFP-actin expressing cells did not significantly decrease in number within this time interval.

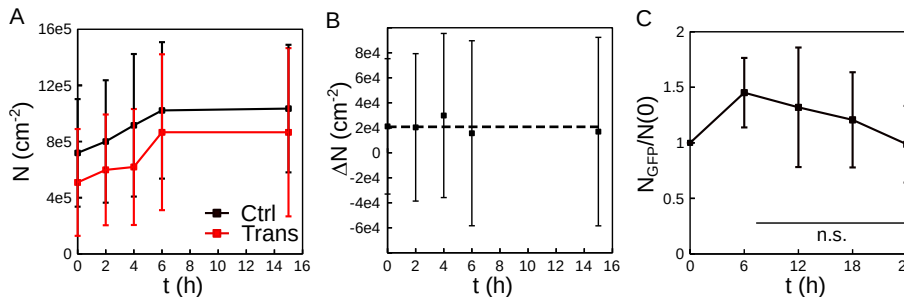


Figure 2: Effect of gene transfer on cell proliferation on 3.5 kPa hydrogel. (A) Mean of the cell density in the transduced (in red) and control conditions (in black) on 3.5 kPa gel. (B) The difference in cell density between the control and the transduced conditions does not significantly evolve in time. The dashed line is the mean value in time (Student test around the mean: $p = 0.001$). (C) The normalized number of fluorescent cells remains constant (Student test around the mean: $p = 1$). Time $t = 0$ is the beginning of the experiments, 20 h post seeding. n.s.: non significant. Bars show the standard deviations of the repeats ($n = 4$, 3564 and 5036 cells for the transduction and control conditions in A–B, 1267 cells in C).

3.3. The distribution of cell-substrate contact areas is affected by the gene transfer although they are unchanged on average

Cells transmit forces to the substrate through their surface of contact. In single cell conditions, cell geometry was shown to affect cellular forces [Oakes et al. \(2014\)](#). To the best of our knowledge, this effect was not investigated at higher cell density. We nevertheless suspected that a variation in cell contact area may also influence cellular forces for densities that are relevant for epithelial cell culture. In this context, we investigated whether cell contact area would be altered by the transduction. This analysis was conducted on cell monolayers grown on soft hydrogels (3.5 kPa). The transduction assays were performed on the hydrogel, 6 h post seeding. As shown on Figure 1E, the transduction rate of the cells grown on 3.5 kPa with collagen 1 coating at $1 \mu\text{g}/\text{cm}^2$ was of order of 12% for a seeding density of 60000 cells/ cm^2 . This low proportion of cells with a noticeable level of fluorescence did not correspond to the presence of several stained cells in any field of view at the large magnification that is required for mechanical stress analysis, leading to a risk of selection bias. We thus increased the seeding density, but this accordingly reduced the transduction efficiency, as anticipated by the manufacturer. The best compromise was to work with seeding densities spanning from 80000 to 100000 cells/ cm^2 and limit the duration of the experiment to prevent the formation of multilayers. Because of this technical limitation, images were captured 25 h to 30 h post seeding. Although two seeding densities were tested, only monolayers with immature junctions were presumably formed, as suggested by the irregular cell shapes. Parallel experiments were conducted: the cells were seeded at identical cell density in the control and the transduced conditions. Images were acquired for the control condition, and after a delay for the transduced condition. This protocol was designed to compensate for the delay in cell proliferation induced by the transduction process that we have reported above. Thus images were captured at similar cell densities in both conditions, assessed by a rough estimate of cell crowding on phase contrast images. In the following, we refer to cells that have been exposed to the transduction medium as transduced cells, although they may not express GFP-actin.

We then measured the contact surface of the cells with the substrate. This area thus includes cryptic lamellipodia (Fig. S3). In the denser parts of the monolayers, the contact area was occasionally smaller than the size of the nucleus. In these situations, the nucleus was laying on top of neighboring cells while a cellular extension was spread on the substrate. This 3D organization was taken into account by analyzing multiple depths in stacks of images both in phase contrast and fluorescence channels. A first observation is that there is no significant influence of gene transfer on the mean cell contact area

(Fig. 3A). Nevertheless, the cumulative distribution of contact areas from the total number of cells (336 control cells, 332 transduced cells) reveals a significantly larger proportion of large contact areas in the transduced condition, compared to the control (Fig. 3B, KS test: $p < 0.001$).

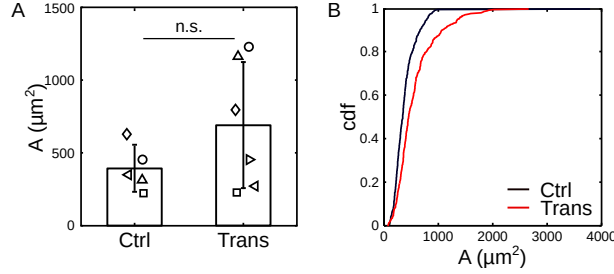


Figure 3: Effect of gene transfer on cell-substrate contact area. (A) The mean contact area of the cells is not sensitive to transduction ($p = 0.17$). (B) The cumulative distribution (cdf) of contact areas of the transduced cells is shifted to larger values (KS test, $p < 0.001$). Bars show the standard deviations of the repeats and the symbols in A show the medians of the independent experiments. Identical symbols for the control and the transduced conditions are used for paired experiments (336 and 332 cells for the control and transduction conditions). n.s. denotes non significant.

3.4. GFP-actin transduction slightly alters cellular forces in immature monolayers

To investigate potential transduction-induced alteration of cellular stresses, we assayed parallel control and transduction experiments, as described above. Traction forces were calculated using Fast Fourier Transformation (Butler et al., 2002). An example of a surface force map is shown in Fig. 4C. A qualitative comparison of the control and the transduced conditions did not show specific force patterns that could differentiate both conditions (Fig. S4). Would the transduction be without side effects, the parallel experiments should give cellular stresses of similar magnitudes. We therefore tested the null hypothesis, that the traction forces are identical between the two set of samples using a unilateral paired Student test. We obtained that cells that have undergone the transduction process exert on average tensile forces similar to those of untreated control cells (Fig. 4E, $p = 0.91$). Cumulative distributions nevertheless showed a significant shift toward higher tensions (Fig. 4F, $p = 0.01$). Since in transduced condition there are cells with larger contact area with the substrate than in the control (Fig. 3), we wondered whether the population of transduced cells at the origin of the higher tensile forces is the population with larger contact area. No correlation between cell tensile forces and contact area could be observed for either the transduced or the control conditions (Fig. 4G, Spearman’s rank correlation test: $p_{Trans} = 0.47$, $p_{Ctrl} = 0.94$). Nevertheless, the surface forces of the transduced and the control conditions showed a slightly significant, constant difference when comparing cells of similar contact area (Fig. 4H, Student test around the mean, $p = 0.05$).

We next asked whether this difference in the surface forces could be related to a difference in intracellular stress generation. We thus measured the areal strain that results locally from the cell contractile activity, which expresses simply in terms of the substrate displacement field $\mathbf{u} = (u_x, y_y)$, with $\epsilon_a = \partial_x u_x + \partial_y u_y$. We plot this quantity in Fig. 4D and Fig. S4. Integrated over the cell area, areal strain provides a cell-scale indicator of the contraction incurred by the underlying substrate due to the cellular activity,

$$\frac{\Delta A}{A} = \frac{1}{A} \int_A \epsilon_a dx dy \quad (2)$$

The mean value of the stress-induced cell areal strain (Eq. 2) was however not significantly modified by the transduction (Fig. 4I, $p = 0.39$), nor was its cumulative distribution (Fig. 4J–K, $p = 0.12$).

3.5. Tensile forces are enhanced by GFP-actin transduction at subconfluent cell density but cell areal strain is not

We have shown above that in monolayers, baculoviral actin transduction only slightly alters the mechanical properties of MDCK cells by increasing the proportion of cells with high tensile stresses. We

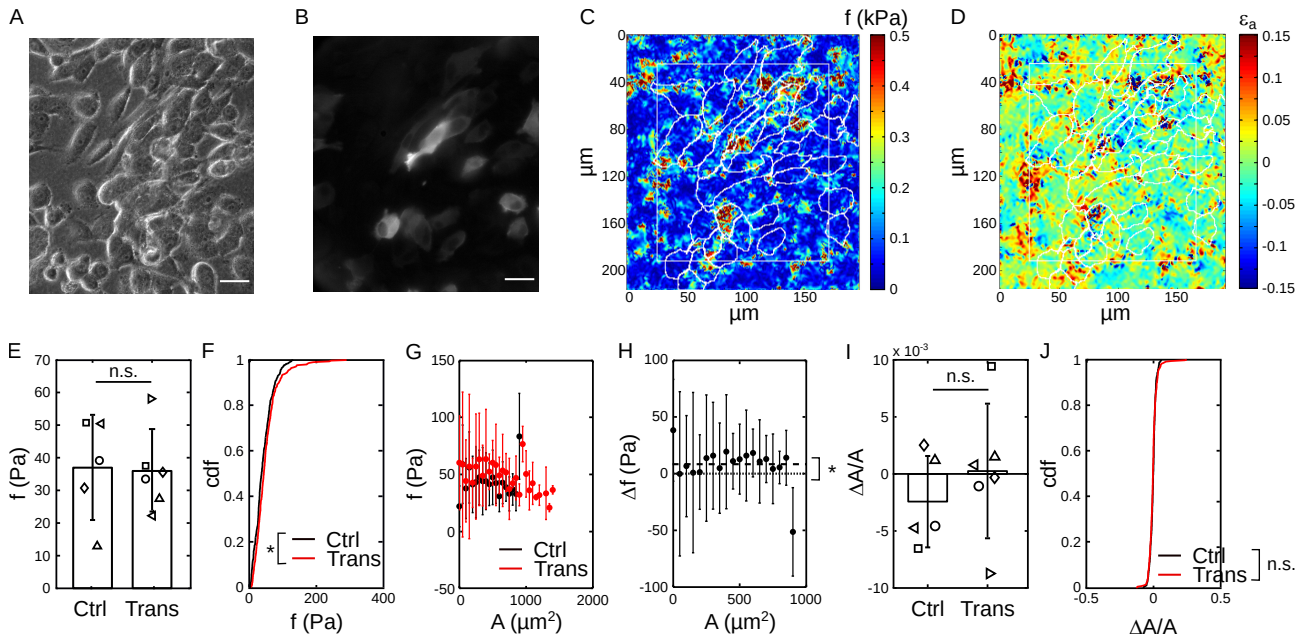


Figure 4: Effect of transduction on cellular stresses. (A) Phase contrast image and (B) fluorescent signal of GFP-actin transduced cells. Bars $25 \mu\text{m}$. (C) Magnitude of the traction forces. The white lines delineate some cellular contours and the corona outside which TFM is not valid. (D) Areal strain. Blue (resp. red) corresponds to contracting (resp. expanding) zones. (E) Mean values of the traction forces for the control and transduced conditions (Student’s test, $p = 0.91$). (F) Cumulative distribution functions are significantly different (KS test, $p = 0.01$). (G) The traction forces do not correlate with cell-substrate contact area for both conditions (Spearman’s rank correlation test: $p_{Trans} = 0.47$, $p_{Ctrl} = 0.94$). (H) The difference in surface force between the transduction and the control conditions distributes around a non zero constant (Student test around the mean, $p = 0.05$). (I) The means of the relative changes in cell contact area due to cellular stresses (Eq. 2) are not significantly different (Student test, $p = 0.39$), (J) nor their cumulative distribution functions (KS test, $p = 0.12$). In E and I, bars are the standard deviations of the repeats and the symbols show the medians of the independent experiments. Identical symbols show paired experiments (336 and 332 cells for the control and transduction conditions). Bars show the standard deviations from the cells in the other graphs. * and n.s. denote respectively $p < 0.05$ and non significant.

wondered whether the effect of the transduction is sensitive to cell density. This question arises because increased asymmetry in cell shape was shown to result in greater cellular forces (Oakes et al., 2014). In this context, the seeding density was reduced to 60000 cells/cm^2 , which resulted in subconfluent conditions thus enabling cell/cell contacts but making cell/substrate contact surface comparable to cell area (Fig. S4A–B). In addition to cell contact area and mechanical read-outs, we measured cell eccentricity from the contour of the cell/substrate contact area to get information on cell asymmetry. As expected, cells statistically displayed larger contact area in these subconfluent conditions (compare Fig. 3A and Fig. 5A), but as for higher density, the transduction process did not affect the mean cell contact area (Fig. 5A, $p = 0.89$). Nevertheless, similar to the high density case, comparison of the cumulative distribution functions shows that the transduction process increases the proportion of cells with a large surface area in contact with the substrate (Fig. 5B, $p < 0.001$). In contrast, cell shape, measured by the eccentricity of the cell-substrate contact area, was statistically insensitive to the transduction. Both the mean of the medians of eccentricity measured in independent experiments and the cumulative distribution functions were indistinguishable (Fig. S5C–D, Student test: $p = 0.89$, KS test: $p = 0.64$). Nevertheless, as transduced cells could be larger than the control, we investigated whether these cells could be more elongated, which in turn might affect cellular forces. We first analyzed the relation between cell eccentricity and cell area (Fig. S5E). Cells from the control condition demonstrated a positive correlation between their shape asymmetry and surface area while the transduced cells did not (Spearman’s test: $p_{Ctrl} = 0.04$ for $r = 0.2$, $p_{Trans} = 1$). This correlation suggests that the eccentricity of untreated cells increases with cell surface area, meaning that larger cells are statistically more elongated than the small ones, a trend that is not observed for

treated cells. Altogether, these observations suggest that the gene transfer protocol statistically preserves cell shape symmetry but this statistical observation hides the fact that cell perturbation is dependent on cell area.

As above, we analyzed whether the transduction process entails alterations of the surface forces and the areal strain in subconfluent conditions. A significant difference of the mean of the surface forces was observed (Fig. 5C, $p = 0.02$). Cumulative distributions also showed a significant shift toward high tensions (Fig. 5D, $p < 0.001$). This significant increase of the mean surface force did not reliably relate to a significant increase of the mean cell areal strain (Fig. 5E, $p = 0.82$). However, cumulative distribution functions consistently showed that the transduction process shifts the areal strain to larger amplitudes, suggesting the presence of more contractile or expanding cells. This increase of the mechanical stresses could not be reliably related to a specific subpopulation of cells, for instance in relation to cell area (data not shown).

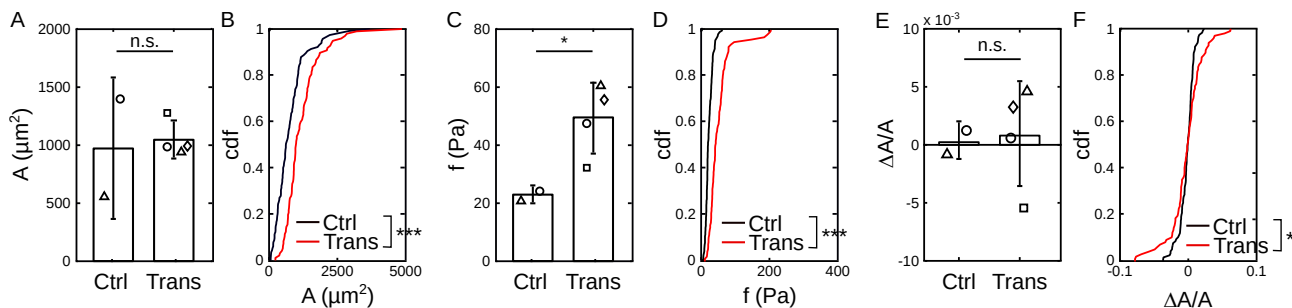


Figure 5: Effect of transduction on cellular stresses for subconfluent cells. (A) The mean cell contact area is not sensitive to transduction ($p = 0.89$). (B) The cumulative distribution of transduced cell area is shifted to larger values (KS test, $p < 0.001$). (C) Mean values of the traction forces for the control and transduced conditions (Student test, $p = 0.02$), and (D) cumulative distribution functions (KS test: $p < 0.001$). (E) The mean areal stress is not sensitive to transduction ($p = 0.83$). (F) The cumulative distribution functions however show a significant shift toward more active cells (KS test: $p = 0.03$). Bars show the standard deviations of the repeats and the symbols in A, C and E show the medians of the independent experiments. Identical symbols for the control and the transduced conditions are used for paired experiments (115 and 97 cells for the control and transduction conditions). *, **, *** and n.s. denote respectively $p < (0.05, 0.01, 0.001)$ and non significant.

3.6. Neither cellular stresses, area or eccentricity are correlated with the level of GFP-actin expression.

Variation in the expression level of GFP-actin correlates with additional synthesis of fluorescent actin, and thus potentially perturbs cellular stresses or morphology. We thus wondered whether for baculoviral transduction, the expression level of GFP-actin correlates with these read-outs. To this end, we analyzed the relation between surface area, eccentricity, traction forces, and contractility-induced cell areal strain with the intensity level per unit cell area (Fig. 6A–D). Note that here, the data from different fields of view could not be pooled since the reference intensity was different in the different acquisitions. We therefore performed correlation analysis on each field of view, and obtained the probability that data correlate with the intensity per unit cell area from Spearman’s correlation rank tests. The distribution of the p-values were then analyzed. None of the parameters of focus appeared sensitive to the expression level of GFP-actin (Fig. 6E). Data were indeed randomly distributed around a mean value, dependent on the field of view (Fig. 6A–D).

4. Discussion

Using a commercial baculoviral transduction method for actin live staining (BacMam, CellLight® actin-GFP), we investigated the impact of the transduction on the mechanical behavior of MDCK cells, an epithelial cell model. Here we focused on transduction-induced disturbance of the cellular stresses, monitored through the traction forces the cells transmit to the extracellular matrix and the area changes

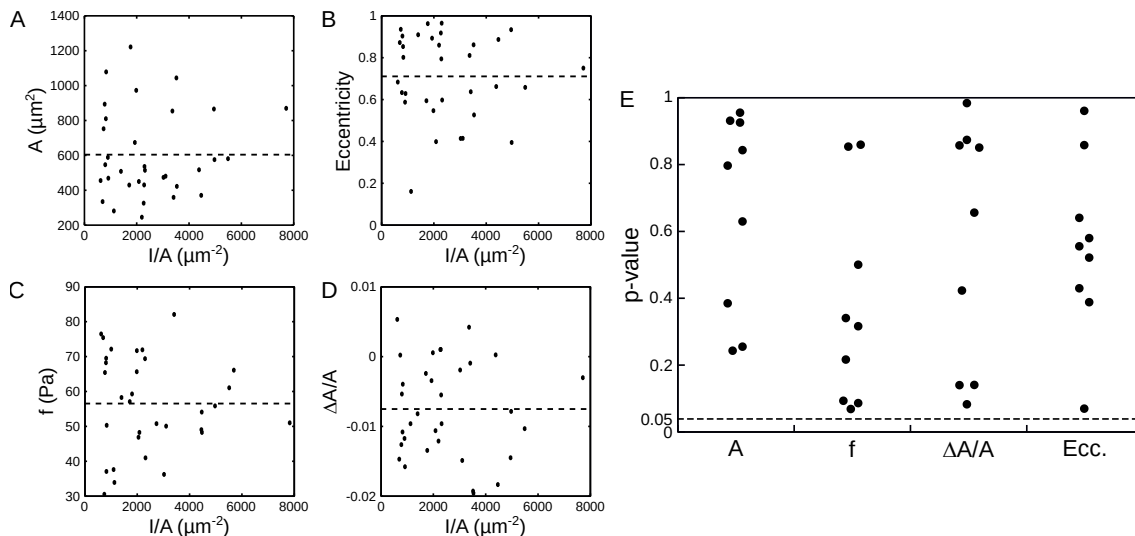


Figure 6: Neither cell-substrate contact area, eccentricity, traction forces nor the cell areal strain are significantly influenced by the expression level of GFP-actin. (A–D) Example of the relations between contact area (A), eccentricity (B), traction forces (C) and cell areal strain (D) with the fluorescent intensity per unit cell area for a given field of view. Dashed lines show the mean values. Data distribute randomly around the mean (Student tests: $p_A = 0.9$, $p_{\Delta A/A} = 0.6$, $p_f = 0.5$, $p_{Ecc.} = 0.4$). (E) p -values from Spearman’s rank correlation tests calculated in each field of view (9 fields of view from 3 experiments, 280 cells). All p -values are above 0.05, leading to reject the hypothesis of a correlation of expression level of GFP-actin with each of the readouts in each of the fields of view.

that result from internal contractility. To the best of our knowledge, previous studies devoted to mechanical alterations of cells induced by live staining have focused on cell rheological properties (Deibler et al., 2011; Pravin Kumar et al., 2012; Sliogeryte et al., 2016; Nagasaki et al., 2017; Flores et al., 2019). However, the relation between cellular stresses and cell stiffness is not straightforward. E.g., well organized actin stress fibers might provide a large cellular stiffness while applying forces that are less than those from less organized actin filaments (Murrell et al., 2015). Since cellular stresses are often a key quantity in biophysical assays involving live actin staining, a direct assessment of the impact of staining on cellular stress is of first importance. To this end, we have compared cellular stresses from transduced cells and from cells that have not been exposed to the transduction process (named untransformed or control cells hereafter). Doing so, we could conclude on the side effects of this transduction process on cell mechanics, that could either be due to a potential variation of the actin expression or to cell alteration originating from the transduction technology itself. This information is very valuable when cellular forces are used as a read-out in live systems in which actin staining is being used, as was done for example in some major studies in mechanobiology (Wolfenson et al., 2016; Oakes et al., 2014; Doss et al., 2020). With this choice of control condition, we intentionally did not focus on the molecular mechanisms of transduction and potential side effects such as changes in actin expression. Our focus was on quantifying how this transduction method biases or does not bias the mechanical measurements.

Stress measurements were performed on soft matrices, with Young’s modulus in the range of cells Young’s moduli, of order of the kPa (Mulligan et al., 2018). We first tested the efficacy of GFP-actin transduction in dependence on the stiffness of the extracellular matrix. Previous work had shown that poly(ethyleneimine) transfer of gene exhibited reduced gene expression on softer substrates (Kong et al., 2005). We observed that in MDCK cell line, the expression level resulting from the transduction in adhered cells was not sensitive to stiffness (Fig. 1F). We additionally observed that the percentage of fluorescent cells was larger on the soft matrix (Fig. 1E). This observation differs from the one of a previous study (Missirlis, 2014) that reported a stiffness-independent percentage of transfected cells. The latter result was obtained using a chemical transfection process involving clathrin-dependent endocytosis. The difference with our observation could arise from the different endocytosis process that takes place in

BacMam transduction, as not all the endocytosis processes show identical stiffness sensitivity (Missirlis, 2014). For instance, baculoviral uptake is suspected to be driven by lipid-raft mediated endocytosis (Laakkonen et al., 2009), that was shown to be stiffness insensitive (Missirlis, 2014). Then, cell density which also impacts the efficacy of gene transduction becomes a major limitation for the cellular uptake of the vector. Indeed, cell proliferation was slower on the softer matrix (Fig. 1D), as already reported for other normal cell types (Peyton et al., 2006).

Traction forces are known to depend on cell shape (Oakes et al., 2014) and cell density (Venugopal et al., 2018). Here we qualitatively addressed stress dependence on cell density. Two situations were analyzed: subconfluent density, where the cells are not packed and cell shape resembles single cell shape; and dense cultures, where cell spreading is obviously constrained by the presence of neighbors. As MDCK cells are epithelial cells, our initial goal was to reach mature epithelial monolayers. We nevertheless did not attain this mature state because the transduction efficiency was not sufficient to reach maturity while keeping a proportion of fluorescent cells above 10 % per field of view at the large magnification that is required for precise traction force quantification. At high cell density, the impact of the transduction was thus analyzed on immature monolayers. To reach immature monolayers, cell seeding density was varied from 80000 to 100000 cells/cm². The data from both these seeding densities were pooled as experiments did not show any significant difference for all the parameters that we quantified (data not shown). This observation is not surprising as epithelial cells were grown from cellular clusters, the local cell density being highly non uniform.

Our main finding is that baculoviral GFP-actin transduction has a complex impact on cellular stresses that is enhanced at lower cell density (Fig. 4 and Fig. 5). At high cell density, the transduction hardly altered cellular surface forces. Surface forces obtained from 5 independent experiments implying more than 300 cells per condition showed mean values that were unchanged by the transduction (Fig. 4E). The cumulative distribution functions nevertheless showed an increased proportion of cells that exert higher surface forces in the transduced condition (Fig. 4F). This effect was enhanced at lower cell density (Fig 5C–D). The proportion of cells that exert higher surface stresses was noticeably increased, and the mean of the surface forces in the transduced condition was significantly shifted toward larger value compared to the control, untransformed cells (Fig. 5C).

As an alternative to the comparison of traction forces, we quantified and compared the areal strain, that is the change in cell surface area that would result from a gedanken experiment in which adherent cells would move from a relaxed to a tensed state (Delanoë-Ayari et al., 2022; Delanoë-Ayari and Nicolas). The strain tensor at the basal surface of the cell was calculated using the ISM approach (Moussus et al., 2014a) (Eq. 1), which allowed to deduce the relative variation in cell basal area resulting from intracellular stresses (Eq. 2). This read-out showed less sensitivity to the transduction process than the traction forces but shared the same trends. No difference in the mean values of the areal strain of the control and the transduced conditions nor in their cumulative distribution functions were found at large cell density (Fig. 4I–J). At lower densities however, the cumulative distribution function of the areal strain of the transduced cells revealed a significant proportion of cells with a higher level of intracellular strain, evenly distributed between more contractile and more expansive cells (Fig. 5F).

Inspired by the observation that single cells geometry correlates with traction forces (Oakes et al., 2014), we measured the impact of the transduction process on cell morphology. We investigated first whether the contact area of the cells with the substrate correlates with traction forces or areal strain for epithelial cells with intercellular contacts, and secondly whether the transduction process may influence it. In contrast with single cells (Oakes et al., 2014), we did not observe any correlation between cell surface forces (or areal strain) and cell contact surface in both conditions of cell densities tested (Fig. 4G and Fig. S5A–B). This result is not surprising when the cell density is high, because in this case the contact surface can differ considerably from the projected surface of the cells: the cells are interwoven, with lamellipodia extending underneath neighboring cells or contacting the substrate only by part of their projected surface. At lower cell density however, the contact and the projected areas are very similar. Our observation therefore suggests that cell/cell contacts may impact the positive correlation

that is reported for single cells. Nevertheless, we consistently observed at subconfluent cell density that the eccentricity of cell shape positively correlates with traction forces, meaning that the more the cells are elongated, the stronger the surface forces they transmit to the substrate (Fig. S5E). Concerning the influence of the transduction process on cell morphology, we obtained that the mean cell-substrate contact area is insensitive to it for both conditions of cell density (Fig. 3A, 5A and S5C), but the cell population previously exposed to the transduction medium exhibited some larger cells in both cases (Fig. 3B and Fig. 5B). Nevertheless, while the transduction process leads to the emergence of larger cells, no correlation of the contact area with cellular stresses was observed (Fig. 4G and Fig. S5A–B). The cells that were previously exposed to the transduction medium also did not exhibit any correlation between cell asymmetry and surface forces (Fig. S5E).

The subtle changes in cell shape following baculoviral transduction are to be compared to LifeAct transduction (Flores et al., 2019; Sliogeryte et al., 2016). LifeAct transduction was shown to induce significant morphological changes in cells, in a dose dependent manner and in correlation to the expression level. The impact of the baculoviral transduction on cell shape seems more limited, as it only affects a small population of cells independent of the expression level of GFP-actin (Fig. 6A–B). Although the impact of LifeAct transduction on cellular stress has not yet been addressed, it is expected that the significant change in shape that is reported will in turn also imply changes in cellular stress in the same way as we report changes for baculoviral transduction.

The endeavor to understand such cell mechanics necessitates visualization tools such as live actin staining which, ideally, should leave rheological and morphological properties unaffected as well as cell contractile activity. While there are currently no techniques which would perfectly match this criterion, our study takes part in a broader effort to characterize the side effects of such stainings. For instance, Pravincumar et al. (2012) showed that BacMam actin transduction was fluidizing the cell body of suspended cells. Differently, Sliogeryte et al. (2016); Nagasaki et al. (2017) reported a stiffening of suspended and adherent cells chemically transfected with GFP-actin, while viral transduction of LifeAct staining was not altering cell mechanical properties (Sliogeryte et al., 2016). These studies suggest that BacMam transduction, while also involving GFP-actin gene transfer, does not disrupt cell mechanics in a similar manner as the chemical transfections studied (lipofectamin and poly(ethyleneimine)). Consistent with this, no correlation was found between the increase of cellular stresses for cells that have been exposed to the transduction medium and the expression level of GFP-actin (Fig. 6E). It was shown that an appropriate position of the GFP coding sequence in the transferred gene is important to minimize impact on cell mechanics (Nagasaki et al., 2017). Here, we show that in addition to the engineering of the gene itself, the choice of the technology of gene transfer is of primary importance.

5. Conclusions

In conclusion, we proposed for the first time an analysis of the influence of baculoviral GFP-actin transduction on cellular stresses for adherent epithelial cells. We observed that the transduction affects cell mechanical response by increasing the proportion of cells with large stresses, equally distributed between tensile and extensile cells. This effect appeared more marked at subconfluent cell density. The increase in stress was accompanied by a small but complex disturbance in cell morphology, that did not correlate with cell area. Although it only marginally affects cell morphology, this live staining method of actin therefore turns out to bear some limitations for the mechanical analysis of cell behaviour. This would not have been anticipated if limiting the analysis to perturbations in cell morphology. Studying the influence on cellular stresses of the other techniques of actin live staining could help controlling bias in studies of adherent cell mechanics.

Acknowledgments

The authors are indebted to H. Delanoë-Ayari for sharing TFM codes. The authors acknowledge D. Gulino-Debrac and C. Migdal for critical reading. This work was partly supported by the french Renatech

network and by the French National Research Agency in the framework of the "Investissements d'avenir" program (ANR-15-IDEX-02).

Authors contribution

S. B.: Investigation, Formal analysis. J. E.: Funding acquisition, Supervision, Conceptualization, Writing original draft. A. N.: Conceptualization, Methodology, Formal analysis, Visualization, Supervision, Funding acquisition, Project administration, Writing original draft. All authors have read and commented on the manuscript.

Funding

This work is supported by the French National Research Agency in the framework of the "Investissements d'avenir" program (ANR-15-IDEX-02).

Conflict of interest

A.N. is co-founder, shareholder and scientific advisor of Cell&Soft company that sells pre-coated soft hydrogels for cell culture with uniform or textured stiffness.

References

- Aizawa, H., Sameshima, M., Yahara, I., 1997. A green fluorescent protein-actin fusion protein dominantly inhibits cytokinesis, cell spreading, and locomotion in dictyostelium. *Cell Struct. Funct.* 22, 335–345. doi:[10.1247/csf.22.335](https://doi.org/10.1247/csf.22.335).
- Belin, B.J., Goins, L.M., Mullins, R.D., 2014. Comparative analysis of tools for live cell imaging of actin network architecture. *BioArchitecture* 4, 189–202. doi:[10.1080/19490992.2014.1047714](https://doi.org/10.1080/19490992.2014.1047714). PMID: 26317264.
- Butler, J.P., Tolic-Nørrelykke, I.M., Fabry, B., Fredberg, J.J., 2002. Traction fields, moments, and strain energy that cells exert on their surroundings. *Am. J. Physiol. Cell Physiol.* 282, C595–C605. doi:[10.1152/ajpcell.00270.2001](https://doi.org/10.1152/ajpcell.00270.2001).
- Chen, C.Y., Lin, C.Y., Chen, G.Y., Hu, Y.C., 2011. Baculovirus as a gene delivery vector: recent understandings of molecular alterations in transduced cells and latest applications. *Biotechnol. Adv.* 29, 618–631. doi:[10.1016/j.biotechadv.2011.04.004](https://doi.org/10.1016/j.biotechadv.2011.04.004).
- Deibler, M., Spatz, J.P., Kemkemer, R., 2011. Actin fusion proteins alter the dynamics of mechanically induced cytoskeleton rearrangement. *PLoS One* 6, e22941. doi:[10.1371/journal.pone.0022941](https://doi.org/10.1371/journal.pone.0022941).
- Delanoë-Ayari, H., Bouchonville, N., Courçon, M., Nicolas, A., 2022. Linear correlation between active and resistive stresses provides information on force generation and stress transmission in adherent cells. *Phys. Rev. Lett.* 129, 098101. doi:[10.1103/PhysRevLett.129.098101](https://doi.org/10.1103/PhysRevLett.129.098101).
- Delanoë-Ayari, H., Nicolas, A., . Quantifying active and resistive stresses in adherent cells 106, 024411. doi:[10.1103/physreve.106.024411](https://doi.org/10.1103/physreve.106.024411).
- Doss, B.L., Pan, M., Gupta, M., Greci, G., Mège, R.M., Lim, C.T., Sheetz, M.P., Voituriez, R., Ladoux, B., 2020. Cell response to substrate rigidity is regulated by active and passive cytoskeletal stress. *Proc. Natl Acad. Sci. U.S.A.* 117, 12817–12825. doi:[10.1073/pnas.1917555117](https://doi.org/10.1073/pnas.1917555117).

- Dupont, S., Morsut, L., Aragona, M., Enzo, E., Giulitti, S., Cordenonsi, M., Zanconato, F., Le Digabel, J., Forcato, M., Bicciato, S., Elvassore, N., Piccolo, S., 2011. Role of yap/taz in mechanotransduction. *Nature* 474, 179–183. doi:[10.1038/nature10137](https://doi.org/10.1038/nature10137).
- Evers, T.M.J., Holt, L.J., Alberti, S., Mashaghi, A., 2021. Reciprocal regulation of cellular mechanics and metabolism. *Nature Metab.* 3, 456–468. doi:[10.1038/s42255-021-00384-w](https://doi.org/10.1038/s42255-021-00384-w).
- Flores, L.R., Keeling, M.C., Zhang, X., Sliogeryte, K., Gavara, N., 2019. Lifeact-taggef2 alters f-actin organization, cellular morphology and biophysical behaviour. *Sci. Rep.* 9, 3241. doi:[10.1038/s41598-019-40092-w](https://doi.org/10.1038/s41598-019-40092-w).
- Hu, Y.C., 2008. Baculoviral vectors for gene delivery: a review. *Curr. Gene Ther.* 8, 54–65. doi:[10.2174/156652308783688509](https://doi.org/10.2174/156652308783688509).
- Hur, S.S., del Álamo, J.C., Park, J.S., Li, Y.S., Nguyen, H.A., Teng, D., Wang, K.C., Flores, L., Alonso-Latorre, B., Lasheras, J.C., Chien, S., 2012. Roles of cell confluency and fluid shear in 3-dimensional intracellular forces in endothelial cells. *Proc. Natl Acad. Sci. U.S.A.* 109, 11110–11115. doi:[10.1073/pnas.1207326109](https://doi.org/10.1073/pnas.1207326109).
- Iwamoto, D.V., Calderwood, D.A., 2015. Regulation of integrin-mediated adhesions. *Curr. Opin. Cell Biol.* 36, 41–47. doi:[10.1016/j.ceb.2015.06.009](https://doi.org/10.1016/j.ceb.2015.06.009).
- Kong, H.J., Liu, J., Riddle, K., Matsumoto, T., Leach, K., Mooney, D.J., 2005. Non-viral gene delivery regulated by stiffness of cell adhesion substrates. *Nat. Mater.* 4, 460–464. doi:[10.1038/nmat1392](https://doi.org/10.1038/nmat1392).
- Laakkonen, J.P., Mäkelä, A.R., Kakkonen, E., Turkki, P., Kukkonen, S., Peränen, J., Ylä-Herttuala, S., Airene, K.J., Oker-Blom, C., Vihinen-Ranta, M., Marjomäki, V., 2009. Clathrin-independent entry of baculovirus triggers uptake of e. coli in non-phagocytic human cells. *PLoS One* 4, e5093. doi:[10.1371/journal.pone.0005093](https://doi.org/10.1371/journal.pone.0005093).
- Liu, Y., Joo, K.I., Lei, Y., Wang, P., 2014. Visualization of intracellular pathways of engineered baculovirus in mammalian cells. *Virus Res.* 181, 81–91. doi:[10.1016/j.virusres.2014.01.006](https://doi.org/10.1016/j.virusres.2014.01.006).
- Lucas, B.D., Kanade, T., 1981. An iterative image registration technique with an application to stereo vision., in: *Int. Joint Conf. on Artificial Intelligence*, pp. 674 – 679.
- Melak, M., Plessner, M., Grosse, R., 2017. Actin visualization at a glance. *J. Cell Sci.* 130, 525–530. doi:[10.1242/jcs.189068](https://doi.org/10.1242/jcs.189068).
- Mgharbel, A., Migdal, C., Bouchonville, N., Dupenloup, P., Fuard, D., Lopez-Soler, E., Tomba, C., Courçon, M., Gulino-Debrac, D., Delanoë-Ayari, H., Nicolas, A., 2022. Cells on hydrogels with micron-scaled stiffness patterns demonstrate local stiffness sensing. *Nanomaterials* 12, 648. doi:[10.3390/nano12040648](https://doi.org/10.3390/nano12040648).
- Missirlis, D., 2014. The effect of substrate elasticity and actomyosin contractility on different forms of endocytosis. *PLoS One* 9, e96548. doi:[10.1371/journal.pone.0096548](https://doi.org/10.1371/journal.pone.0096548).
- Moussus, M., der Loughian, C., Fuard, D., Courçon, M., Gulino-Debrac, D., Delanoë-Ayari, H., Nicolas, A., 2014a. Intracellular stresses in patterned cell assemblies. *Soft Matter* 10, 2414–2423. doi:[10.1039/C3SM52318G](https://doi.org/10.1039/C3SM52318G).
- Moussus, M., der Loughian, C., Fuard, D., Courçon, M., Gulino-Debrac, D., Delanoë-Ayari, H., Nicolas, A., 2014b. Reply to the 'comment on "intracellular stresses in patterned cell assemblies"' by D. Tamba et al., *Soft Matter*, 2014, 10, 7681. *Soft Matter* 10, 7683–7684. doi:[10.1039/c4sm01066c](https://doi.org/10.1039/c4sm01066c).

- Mulligan, J.A., Bordeleau, F., Reinhart-King, C.A., Adie, S.G., 2018. Traction force microscopy for non-invasive imaging of cell forces. *Adv. Exp. Med. Biol.* 1092, 319–349. doi:[10.1007/978-3-319-95294-9_15](https://doi.org/10.1007/978-3-319-95294-9_15).
- Murrell, M., Oakes, P.W., Lenz, M., Gardel, M.L., 2015. Forcing cells into shape: the mechanics of actomyosin contractility. *Nat. Rev. Mol. Cell Biol.* 16, 486–498. doi:[10.1038/nrm4012](https://doi.org/10.1038/nrm4012).
- Nagasaki, A., Kijima, S.T., Yumoto, T., Imaizumi, M., Yamagishi, A., Kim, H., Nakamura, C., Uyeda, T.Q., 2017. The position of the gfp tag on actin affects the filament formation in mammalian cells. *Cell Struct. Funct.* 42, 131–140. doi:[10.1247/csf.17016](https://doi.org/10.1247/csf.17016).
- Oakes, P.W., Banerjee, S., Marchetti, M.C., Gardel, M.L., 2014. Geometry regulates traction stresses in adherent cells. *Biophys. J.* 107, 825–833. doi:[10.1016/j.bpj.2014.06.045](https://doi.org/10.1016/j.bpj.2014.06.045).
- Oakes, P.W., Bidone, T.C., Beckham, Y., Skeeters, A.V., Ramirez-San Juan, G.R., Winter, S.P., Voth, G.A., Gardel, M.L., 2018. Lamellipodium is a myosin-independent mechanosensor. *Proc. Natl. Acad. Sci. U.S.A.* 115, 2646–2651. doi:[10.1073/pnas.1715869115](https://doi.org/10.1073/pnas.1715869115).
- Palva, S., Joanne, P., Migdal, C., Lopez Soler, E., Hovhannisyan, Y., Nicolas, A., Agbulut, O., 2020. Polyacrylamide hydrogels with rigidity-independent surface chemistry show limited long-term maintenance of pluripotency of human induced pluripotent stem cells on soft substrates. *ACS Biomater. Sci. Eng.* 6, 340–351. doi:[10.1021/acsbiomaterials.9b01189](https://doi.org/10.1021/acsbiomaterials.9b01189).
- Peyton, S.R., Raub, C.B., Keschrums, V.P., Putnam, A.J., 2006. The use of poly(ethylene glycol) hydrogels to investigate the impact of ECM chemistry and mechanics on smooth muscle cells. *Biomaterials* 27, 4881–4893. doi:[10.1016/j.biomaterials.2006.05.012](https://doi.org/10.1016/j.biomaterials.2006.05.012).
- Prager-Khoutorsky, M., Lichtenstein, A., Krishnan, R., Rajendran, K., Mayo, A., Kam, Z., Geiger, B., Bershadsky, A.D., 2011. Fibroblast polarization is a matrix-rigidity-dependent process controlled by focal adhesion mechanosensing. *Nat. Cell Biol.* 13, 1457–1465. doi:[10.1038/ncb2370](https://doi.org/10.1038/ncb2370).
- Pravincumar, P., Bader, D.L., Knight, M.M., 2012. Viscoelastic cell mechanics and actin remodelling are dependent on the rate of applied pressure. *PLoS One* 7, 1–10. doi:[10.1371/journal.pone.0043938](https://doi.org/10.1371/journal.pone.0043938).
- Riveline, D., Zamir, E., Balaban, N.Q., Schwarz, U.S., Ishizaki, T., Narumiya, S., Kam, Z., Geiger, B., Bershadsky, A.D., 2001. Focal contacts as mechanosensors: externally applied local mechanical force induces growth of focal contacts by an mDia1-dependent and ROCK-independent mechanism. *J. Cell Biol.* 153, 1175–1186. doi:[10.1083/jcb.153.6.1175](https://doi.org/10.1083/jcb.153.6.1175).
- Roca-Cusachs, P., Conte, V., Trepats, X., 2017. Quantifying forces in cell biology. *Nature Cell Biol.* 19, 742–751. doi:[10.1038/ncb3564](https://doi.org/10.1038/ncb3564).
- Sliogeryte, K., Thorpe, S.D., Wang, Z., Thompson, C.L., Gavara, N., Knight, M.M., 2016. Differential effects of lifeact-gfp and actin-gfp on cell mechanics assessed using micropipette aspiration. *J. Biomech.* 49, 310–317. doi:[10.1016/j.jbiomech.2015.12.034](https://doi.org/10.1016/j.jbiomech.2015.12.034).
- Tambe, D.T., Croutelle, U., Trepats, X., Park, C.Y., Kim, J.H., Millet, E., Butler, J.P., Fredberg, J.J., 2013. Monolayer stress microscopy: Limitations, artifacts, and accuracy of recovered intercellular stresses. *PLoS One* 8, e55172. doi:[10.1371/journal.pone.0055172](https://doi.org/10.1371/journal.pone.0055172).
- Venugopal, B., Mogha, P., Dhawan, J., Majumder, A., 2018. Cell density overrides the effect of substrate stiffness on human mesenchymal stem cells' morphology and proliferation. *Biomater. Sci.* 6, 1109–1119. doi:[10.1039/c7bm00853h](https://doi.org/10.1039/c7bm00853h).

- Wang, H.B., Dembo, M., Wang, Y.L., 2000. Substrate flexibility regulates growth and apoptosis of normal but not transformed cells. *Am. J. Physiol. Cell Physiol.* 279, C1345–C1350. doi:[10.1152/ajpcell.2000.279.5.C1345](https://doi.org/10.1152/ajpcell.2000.279.5.C1345).
- Wickström, S.A., Niessen, C.M., 2018. Cell adhesion and mechanics as drivers of tissue organization and differentiation: local cues for large scale organization. *Curr. Opin. Cell Biol.* 54, 89–97. doi:[10.1016/j.ceb.2018.05.003](https://doi.org/10.1016/j.ceb.2018.05.003). cell Dynamics.
- Wolfenson, H., Meacci, G., Liu, S., Stachowiak, M.R., Iskratsch, T., Ghassemi, S., Roca-Cusachs, P., O’Shaughnessy, B., Hone, J., Sheetz, M.P., 2016. Tropomyosin controls sarcomere-like contractions for rigidity sensing and suppressing growth on soft matrices. *Nat. Cell Biol.* 18, 33–42. URL: <http://dx.doi.org/10.1038/ncb3277>, doi:[10.1038/ncb3277](https://doi.org/10.1038/ncb3277).
- Yamaguchi, N., Zhang, Z., Schneider, T., Wang, B., Panozzo, D., Knaut, H., 2022. Rear traction forces drive adherent tissue migration in vivo. *Nature Cell Biol.* 24, 194–204. doi:[10.1038/s41556-022-00844-9](https://doi.org/10.1038/s41556-022-00844-9).